Nuclear Instruments and Methods in Physics Research A 765 (2014) 80–90

Contents lists available at ScienceDirect

Nuclear Instruments and Methods in Physics Research A

journal homepage: www.elsevier.com/locate/nima

Development of n$^+$-in-p large-area silicon microstrip sensors for very high radiation environments – ATLAS12 design and initial results

Y. Unno [i,*], S.O. Edwards [a], S. Pyatt [a], J.P. Thomas [a], J.A. Wilson [a], J. Kierstead [b], D. Lynn [b], J.R. Carter [c], L.B.A. Hommels [c], D. Robinson [c], I. Bloch [d], I.M. Gregor [d], K. Tackmann [d], C. Betancourt [e], K. Jakobs [e], S. Kuehn [e], R. Mori [e], U. Parzefall [e], L. Wiik-Fucks [e], A. Clark [f], D. Ferrere [f], S. Gonzalez Sevilla [f], J. Ashby [g], A. Blue [g], R. Bates [g], C. Buttar [g], F. Doherty [g], L. Eklund [g], T. McMullen [g], F. McEwan [g], V. O'Shea [g], S. Kamada [h], K. Yamamura [h], Y. Ikegami [i], K. Nakamura [i], Y. Takubo [i], R. Nishimura [j], R. Takashima [j], A. Chilingarov [k], H. Fox [k], A.A. Affolder [l], P.P. Allport [l], G. Casse [l], P. Dervan [l], D. Forshaw [l], A. Greenall [l], S. Wonsak [l], M. Wormald [l], V. Cindro [m], G. Kramberger [m], I. Mandic [m], M. Mikuz [m], I. Gorelov [n], M. Hoeferkamp [n], P. Palni [n], S. Seidel [n], A. Taylor [n], K. Toms [n], R. Wang [n], N.P. Hessey [o], N. Valencic [o], Y. Arai [p], K. Hanagaki [p], Z. Dolezal [q], P. Kodys [q], J. Bohm [r], M. Mikestikova [r], A. Bevan [s], G. Beck [s], S. Ely [t], V. Fadeyev [t], Z. Galloway [t], A.A. Grillo [t], F. Martinez-McKinney [t], J. Ngo [t], C. Parker [t], H.F.-W. Sadrozinski [t], D. Schumacher [t], A. Seiden [t], R. French [u], P. Hodgson [u], H. Marin-Reyes [u], K. Parker [u], S. Paganis [u], O. Jinnouchi [v], K. Motohashi [v], K. Todome [v], D. Yamaguchi [v], K. Hara [w], M. Hagihara [w], C. Garcia [x], J. Jimenez [x], C. Lacasta [x], S. Marti i Garcia [x], U. Soldevila [x]

[a] School of Physics and Astronomy, University of Birmingham, Birmingham B15 2TT, United Kingdom
[b] Brookhaven National Laboratory, Physics Department and Instrumentation Division, Upton, NY 11973-5000, USA
[c] Cavendish Laboratory, University of Cambridge, JJ Thomson Avenue, Cambridge CB3 0HE, United Kingdom
[d] DESY, Notkestrasse 85, 22607 Hambrug, Germany
[e] Physikalisches Institut, Universitt Freiburg, Hermann-Herder-Str. 3, D-79104 Freiburg, Germany
[f] DPNC, University of Geneva, 24, Quai Ernest-Ansermet, CH-1211 Genve 4, Switzerland
[g] SUPA – School of Physics and Astronomy, University of Glasgow, Glasgow G12 8QQ, United Kingdom
[h] Solid State Div., Hamamatsu Photonics K.K., 1126-1, Ichino-cho, Higashi-ku, Hamamatsu-shi, Shizuoka 435-8558, Japan
[i] Institute of Particle and Nuclear Study, KEK, Oho 1-1, Tsukuba, Ibaraki 305-0801, Japan
[j] Department of Science Education, Kyoto University of Education, Kyoto 612-8522, Japan
[k] Physics Department, Lancaster University, Lancaster LA1 4YB, United Kingdom
[l] Oliver Lodge Laboratory, Department of Physics, University of Liverpool, Oxford St., Liverpool L69 7ZE, United Kingdom
[m] Josef Stefan Institute and Department of Physics, University of Ljubljana, Ljubljana, Slovenia
[n] Department of Physics and Astronomy, University of New Mexico, MSC07 4220, 1919 Lomos Blvd. NE, Albuquerque, NM 87131, USA
[o] Nikhef, Science Park 105, 1098 XG Amsterdam, Netherlands
[p] Department of Physics, Osaka University, Machikaneyama-cho 1-1, Toyonaka-shi, Osaka 560-0043, Japan
[q] Charles University in Prague, Faculty of Mathematics and Physics, V Holesovickach 2, Prague 8, Czech Republic
[r] Academy of Sciences of the Czech Republic, Institute of Physics, Na Slovance 2, 18221 Prague 8, Czech Republic
[s] School of Physics and Astronomy, Queen Mary University of London, London E1 4NS, United Kingdom
[t] SCIPP, University of California, Santa Cruz, CA 95064, USA
[u] Department of Physics and Astronomy, The University of Sheffield, Hicks Building, Hounsfield Road, S3 7RH Sheffield, United Kingdom
[v] Institute of Science and Engineering, Tokyo Institute of Technology, Ookayama 2-12-1, Meguro-ku, Tokyo 152-8551, Japan
[w] Institute of Pure and Applied Sciences, University of Tsukuba, Tsukuba, Ibaraki 305-9751, Japan
[x] IFIC (Centro Mixto CSIC-UVEG), Edificio Investigacion Paterna, Apartado 22085, 46071 Valencia, Spain

ARTICLE INFO

Available online 14 July 2014

Keywords:
Silicon strip

ABSTRACT

We have been developing a novel radiation-tolerant n$^+$-in-p silicon microstrip sensor for very high radiation environments, aiming for application in the high luminosity large hadron collider. The sensors are fabricated in 6 in., p-type, float-zone wafers, where large-area strip sensor designs are laid out

* Corresponding author.
E-mail address: yoshinobu.unno@kek.jp (Y. Unno).

http://dx.doi.org/10.1016/j.nima.2014.06.086

n^+-in-p
P-type
Radiation-tolerant
HL-LHC
PTP

together with a number of miniature sensors. Radiation tolerance has been studied with ATLAS07 sensors and with independent structures. The ATLAS07 design was developed into new ATLAS12 designs. The ATLAS12A large-area sensor is made towards an axial strip sensor and the ATLAS12M towards a stereo strip sensor. New features to the ATLAS12 sensors are two dicing lines: standard edge space of 910 μm and slim edge space of 450 μm, a gated punch-through protection structure, and connection of orphan strips in a triangular corner of stereo strips. We report the design of the ATLAS12 layouts and initial measurements of the leakage current after dicing and the resistivity of the wafers.

1. Introduction

We have been developing n^+-in-p silicon microstrip sensors with p-type silicon wafers aiming for a cost-effective and radiation-tolerant solution for covering an area over 100 m^2 in very high radiation environments. A specific application of such a silicon microstrip sensor is a replacement of the outer part of the inner tracker in the ATLAS detector [1] for the high luminosity large hadron collider (HL-LHC) [2].

The current inner tracker of the ATLAS detector consists of a pixel tracker (Pixels) at radii of 5–12 cm, a silicon microstrip tracker (SCT/Strips) at 30–51 cm (Barrel cylinders) and at 28–56 cm (Endcap discs) and a transition radiation tracker (TRT) at 56–107 cm. The silicon sensor area is 2.7 m^2 and 62 m^2 in Pixels and Strips, respectively. For the HL-LHC, not only the entire inner tracker is to be replaced but also the TRT is to be replaced with Strips [3]. The latest layout of the inner tracker is Pixels at 4–25 cm and Strips at 40–100 cm. The silicon area is 8.2 m^2 and 193 m^2 (122 Barrel and 71 Endcap per m^2), respectively. In both Pixels and Strips, the areas are increased to approximately three times that of the original ATLAS detector.

With the integrated luminosity of 3000 fb^{-1} and a safety factor 2, a number of particles passing through an unit area in the tracker volume has been simulated [4], as shown in Fig. 1. The typical fluences are approximately: 2.2×10^{16} 1 MeV-neutrons equivalent (n_{eq})/cm^2 at 3.7 cm for the Pixels, and 1×10^{15} n_{eq/cm^2} at 31 cm and 5×10^{14} n_{eq/cm^2} at 60 cm for the Strips. Charged particles dominate inside and neutral particles, mainly neutrons, dominate outside a radius of 25 cm. Our goal of the radiation-tolerant silicon microstrip sensor is to cope with a fluence of $\geq 1 \times 10^{15}$ n_{eq/cm^2} and to be robust against both charged and neutral particles.

2. Radiation-tolerant n^+-in-p silicon strip sensors

The sensor of n^+-implant readout in p-type silicon substrate (n^+-in-p) is intrinsically more radiation-tolerant. This is because the p–n junction develops from the readout implants before and after radiation damage as the radiation-induced levels in the silicon band-gap are primarily acceptor states (p-type) [5]. The fact leads to a number of virtues: (1) the sensors can be operated under partially depleted conditions when the full depletion voltage is extremely high after radiation damage; (2) the signals are generated by collecting electrons and are larger, as compared with collecting holes, because of a faster drift velocity and less charge-trapping in silicon; (3) the sensors can be fabricated with mask-processes only on the segmented side and with diffusion processes on the backside, i.e., the so-called "single-side process". The fabrication cost in this case is 30–40% less than the "double-side process" where both sides are processed with masks; (4) the sensors can be robust against handling because of the absence of segmentation and junctions on the backside. Points (1) and (2) are not applicable to p^+-in-n sensors, while they are possibly applicable to n^+-in-n sensors. Points (3) and (4), however, ensure that n^+-in-p single-side process sensors are more cost-effective than n^+-in-n double-side process sensors.

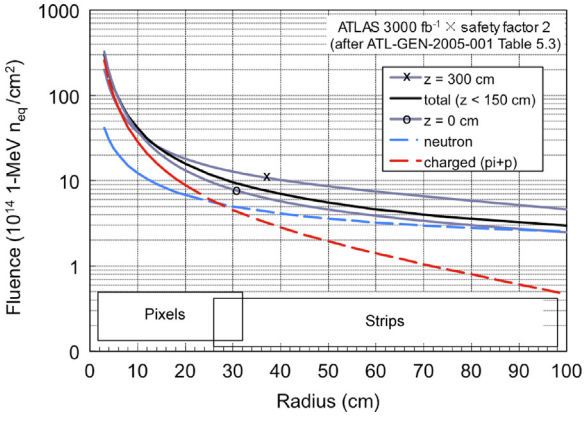

Fig. 1. Expected particle fluences from simulations in the inner tracker of the ATLAS detector for the HL-LHC [4]. The transition from the pixel to the strip detector is at r=(approximately) 30 cm.

2.1. ATLAS07 sensors

We have fabricated large-area strip sensors of 9.75×9.75 cm^2, known as the ATLAS07 sensor, together with 1×1 cm^2 miniature sensors, in 6 in., p-type, float-zone (FZ), 320 μm thick wafers [6]. The large-area main sensor is segmented into four blocks of short strips with a strip length of 2.39 cm each in order to reduce the number of particles simultaneously impinging on a strip (its fraction to total impinging particles known as "occupancy"). Initial evaluation of the ATLAS07 sensors was reported for leakage currents, depletion voltages, and interstrip resistances and capacitances before and after radiation damage [7–10].

Further irradiations have been carried out at CYRIC [11] for 70 MeV and KIT [12] for 23 MeV protons, at PSI [13] for 300 MeV pions, and at Ljubljana [14] for reactor neutrons. Irradiated samples have been kept cold (~20 °C) and "annealed" by heating approximately 80 min at 60 °C for minimizing radiation damage effect. Charge collection has been measured before and after "annealing", typically on the AliBaVa system [15] using a ^{90}Sr β source. The latest results of collected charges after "annealing" are shown in Fig. 2 for two bias voltages. The fluences of different projectiles and energies are scaled with the non-ionizing energy loss factors (NIEL) [16]. The collected charges at a fluence of 1×10^{15} n_{eq/cm^2} are approximately 14,000 and 17,000 electrons at 500 and 900 V bias voltages, respectively. With a typical input noise of 600-800 e, the signal-to-noise ratios will be ~18–23 and ~21–28, respectively.

2.2. Edge space and punch-through protection (PTP) studies

An edge space in a silicon sensor is a required space to hold a bias voltage but is a dead space. A required edge space was studied in 4×4 mm^2 square diodes independent of the ATLAS07 sensors by varying the space in one edge out of four [17]. An edge space of

450 μm was derived to be the minimum for holding a bias voltage of 1 kV initially and as radiation damage accumulated.

The PTP structure is to protect the AC-coupling capacitor formed with the strip implant and the strip metal when the voltage of the strip implant has departed from the voltage of the strip metal. Such a case would happen, e.g., when an accidental beam splash deposited a very large amount of charge in the silicon bulk, and the resulting current flowing through the bias resistor generated a large voltage drop to the strip implant. The PTP structure creates a short-circuiting current path in parallel to the bias resistor to limit the voltage drop to the strip. A novel concept of "gated" PTP structure was introduced by placing the potential of the bias ring over the PTP gap [18,19]. The "gated" PTP structures were effective to improve the PTP performance [17]. Among the structures studied, the "full-gate" PTP structure was shown to have the smallest onset voltage, the sharpest decrease of resistance and the smallest resistance at saturation.

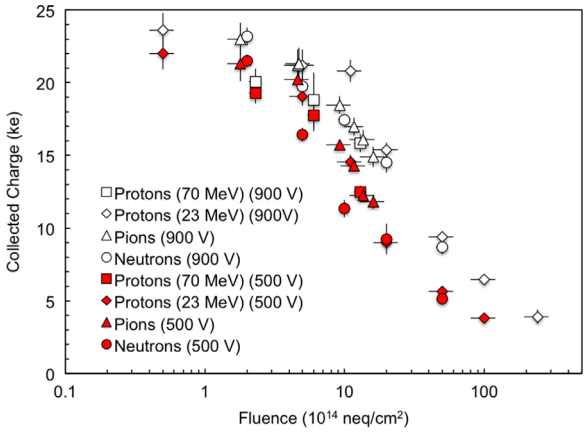

Fig. 2. Collected charges measured by ATLAS07 miniature sensors after radiation damage with 70 MeV (square) and 23 MeV (diamond) protons, pions (triangle), and neutrons (circle) at bias voltages of 500 V (filled) and 900 V (open). The fluences are scaled to a unit of 1-MeV neutrons equivalent/cm^2 using the NIEL factors.

3. ATLAS12 wafer layouts

Developing from the ATLAS07 sensors, we have designed a new set of strip sensors, the ATLAS12A and the ATLAS12M large-area main sensors and miniature sensors in 6-in. wafer. The wafer layouts of the ATLAS12A and the ATLAS12M sensors are shown in Fig. 3. Both ATLAS12A and ATLAS12M large-area main sensors are made to have four "blocks of short strips" (segment). The ATLAS12A main sensor is prototyping an "axial" strip sensor where the strips are running parallel to the sensor edges. The ATLAS12M main sensor is prototyping a "stereo" strip sensor, having "stereo" geometry in the bottom two segments where the strips are inclined to the sensor edges at an angle of 40 mrad. In the peripheral area of each layout, a number of miniature sensors are implemented with variations of the features in the main sensors and with prototypes of the endcap sensors with a fan geometry (see Appendix). Specifications of the ATLAS12 sensors are summarized in Table 1. New features developed from the ATLAS07 into the ATLAS12 main sensor are the implementation of two dicing lines, a gated PTP structure, an arrangement of the wire-bonding pads for the new readout ASIC, and readout of shorter strips in a triangular corner of the stereo layout.

Table 1
Specifications of ATLAS12 n$^+$-in-p large-area silicon microstrip sensor.

Silicon wafer diameter	6 in. (150 mm)
Wafer type	p-type FZ
Crystal orientation	⟨100⟩
Resistivity	>4 kΩ cm (accepting >3 kΩ cm)
Thickness (uniformity)	310 ± 25 μm (± 5 μm)
Number of sections of strip segments	4
Number of strips per section	1282
Strip pitch (θ: stereo angle)	$74.5 \times \cos\theta$ μm
Strip length (θ: stereo angle)	$23.9/\cos\theta$ mm
Angle, θ, of stereo strips	40 mrad
Bias resistance (polysilicon)	1.5 ± 0.5 MΩ
Signal readout	AC coupling
Microdischarge onset voltage	>600 V

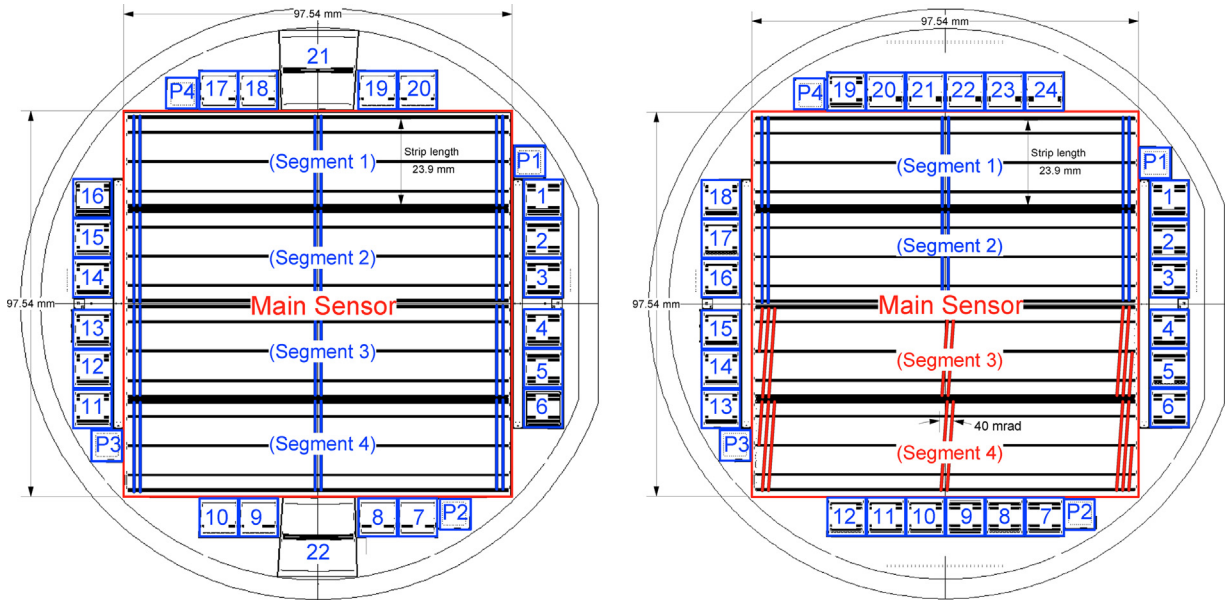

Fig. 3. ATLAS12A (left) and ATLAS12M (right) wafer layout in 6-in. wafer. In ATLAS12A, all four sections of strip segments, 1–4 of the main sensor are made with "axial" strips where the strips are parallel to the sensor edge. In ATLAS12M, the top two strip segments (1 and 2) are "axial" strips and the bottom two (3 and 4) are "stereo" strips where the strips are inclined at an angle of 40 mrad to the sensor edge. The miniature sensors around the perimeter are labeled with the position numbers as 1–24 and the 8×8 mm^2 diodes as P1–P4.

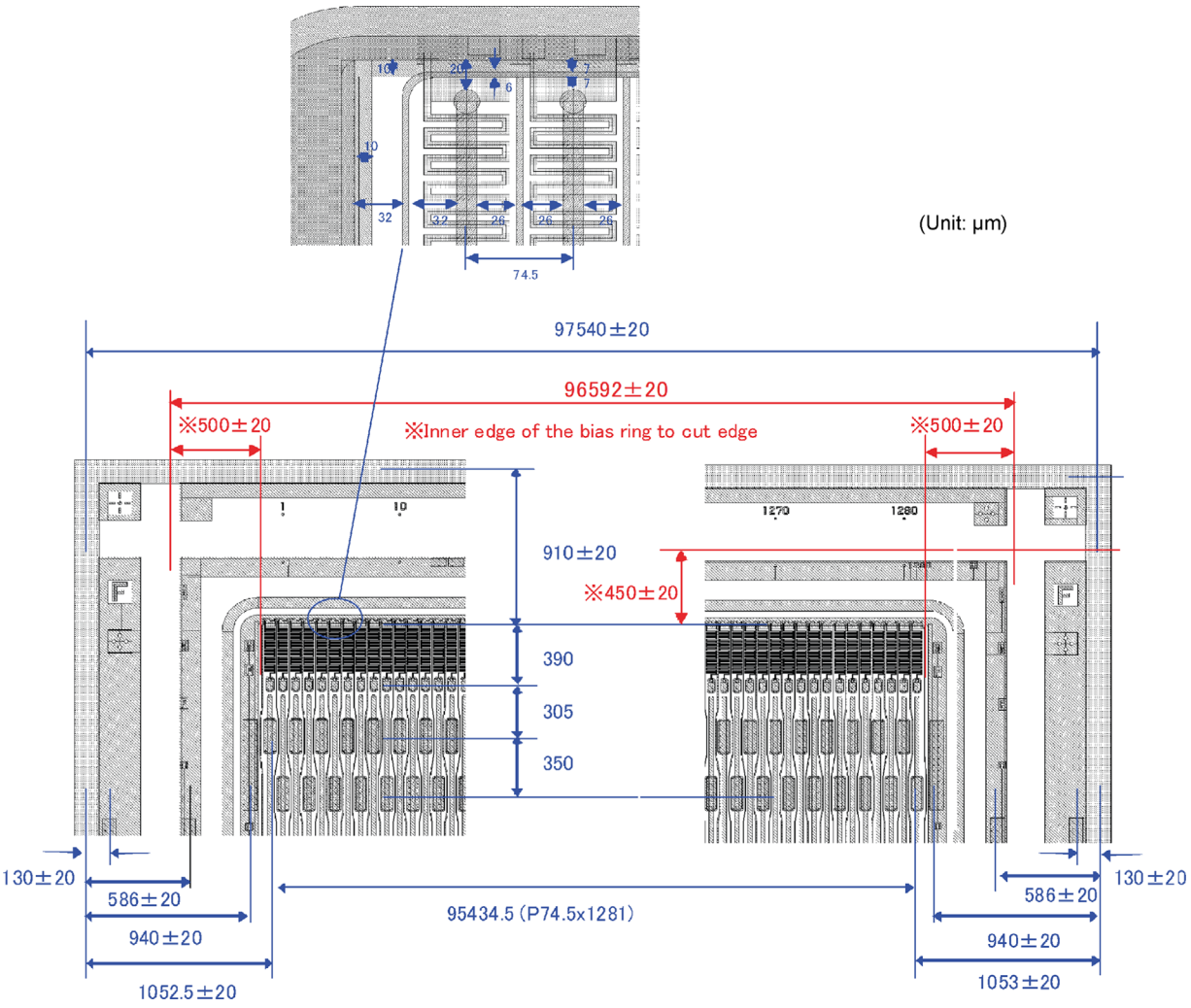

Fig. 4. Dimensions and PTP structure of ATLAS12A and ATLAS12M large-area sensors. The fiducial mark "F" at the corners identifies the orientation of the sensor.

3.1. *"Standard" and "slim" dicing*

The ATLAS07 sensors were made with an edge space of approximately 980 μm (the "standard" to the HPK design). ATLAS12 sensor is designed with two dicing lines, one with the "standard" edge space and the other with the narrow space of approximately 450 μm (the "slim" edge space) in full circumference as shown in Fig. 4. Dicing the sensors with the slim edge space ("slim" dicing) will verify the applicability of the minimum width obtained with the test diodes to a real large-area sensor that have a 100 times longer length in the circumference than the length studied in the diodes.

3.2. *"Full-gate" PTP structure*

The ATLAS07 main sensor had no PTP structures implemented, where the strip-end structure was that of BZ3F in Section A.1. The ATLAS07 miniature sensors had included the PTP structures of BZ3E and BZ4B2 (but without an explicit overlap of the bias resister). No explicit "gated" structure was implemented in the ATLAS07 sensors. The ATLAS12 main sensors are implemented with a "full-gate" structure as shown in the inset of Fig. 4. The ATLAS12 main sensors are the first-time implementation of a "gated" PTP structure in a large area sensor to confirm no adverse effect to the radiation tolerance shown in the ATLAS07 sensors. Variation of "gated" PTP structures is implemented in the miniature sensors of the ATLAS12 layout for understanding the radiation tolerance of the structures further (see Section A.1).

3.3. *Wirebonding pads in strips*

With a new design of 256 channel ASIC, ABCN130 [20], the readout of strips can be arranged so that the strips in two blocks of strips, e.g., the segments 1 and 2 (or 3 and 4) are read out with a single ASIC, as shown in Fig. 5(a). The scheme reduces the number of rows of the ASIC's from 4 to 2, thus reducing the material associated with the ASIC's and the hybrids. Since the pitch of the pads in the ASIC is narrower than the allowed one by the wire-bonding machine, the pads will be separated into 4 rows in the ASIC. The staggering of the pads in the sensor and the ASIC is mirrored so that the wire-bonds can be separated in height. Thus the staggering of the pads in the segments 1 and 2 should be the same. In addition, we design to connect the strips in the segments 1 and 2 to form longer strips. The connection requires the staggering of the pads in the segments 1 and 2 should be mirrored, as shown in Fig. 5(b). A solution is to have triple rows of staggered pads in one of the segments as shown in Fig. 5(c). The rows and staggering of pads in the segments 3 and 4 are 180° rotation-symmetric relative to the segments 1 and 2 to allow rotation of the sensor. The existence of DC-contact pads at the strip ends to test

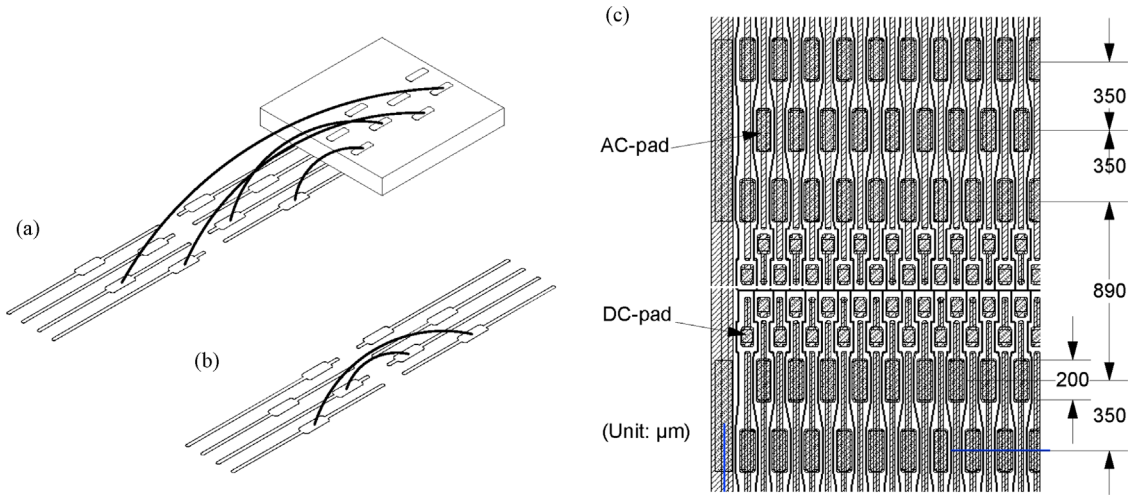

Fig. 5. (a) Wire-bonding between ASIC and strips to readout two segments of strips with one ASIC. (b) Wire-bonding of strips in two segments of strips to form longer strips. (c) A solution of triple rows realized in the main sensor in the strip-segments 1 and 2. AC-pads are those for the wire-bonding that are connected to AC-coupled strip metals. DC-pads are connected to the strip implants directly for quality assurance of the strip implants.

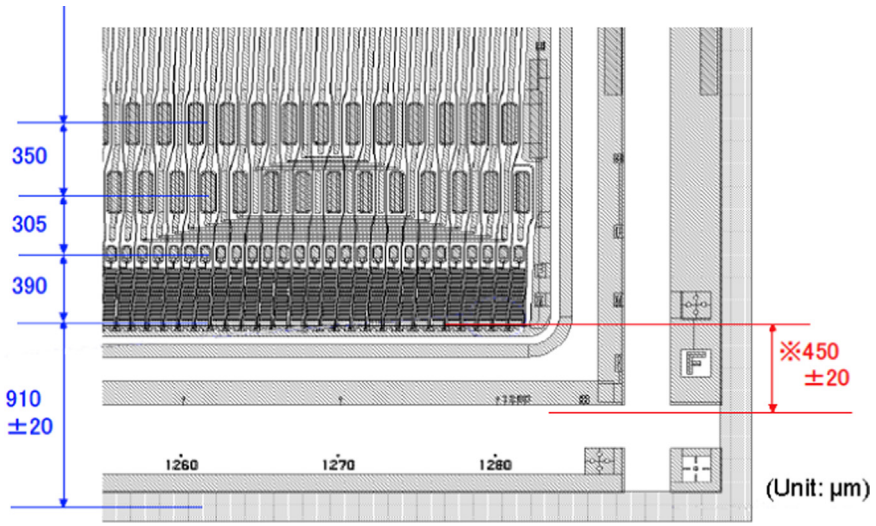

Fig. 6. Connection of orphan strips in the triangular corner of stereo strips that are not connected to readout electronics to readout strips in the segment 4 of ATLAS12M large-area main sensor.

the continuity of n^+ strip implant has constrained the minimum distance of the wire-bonding pads between the segments 1 and 2 (or 3 and 4).

3.4. Connection of orphan strips in the stereo layout

In designing stereo strips in a square sensor there is a triangular corner of shorter strips that may not be connected to readout electronics. Those orphan strips can be readout by connecting the strips to neighbor strips that are connected to readout electronics, the so-called "ganging". Although ganging creates ghosts of space points, the ghosts can be resolved by reconstructing tracks with other layers. A "ganging" is implemented in the ATLAS12M main sensor in the segment 4, being composed of 11 strips as shown in Fig. 6. The connection is made to the AC readout metals in this fabrication (AC-ganging). The connection between strip implants (DC-ganging) is implemented in miniature sensors of endcap geometry (see Section A.2).

4. Initial performance of the ATLAS12 sensors

4.1. Leakage current

The wafer processing of 120 ATLAS12A and 45 ATLAS12M wafers was completed using wafer lots of 6 in., p-type, FZ, and 320 μm thick. Out of these wafers, 30 ATLAS12A and 26 ATLAS12M wafers were diced using stealth dicing technology [21]. For the ATLAS12A dicing, 25 wafers were given standard and 5 slim dicing. For the ATLAS12M, 3 wafers were given standard and 23 slim dicing; thus, in total, 28 standard and 28 slim dicing samples were obtained. The leakage currents as a function of the bias voltage of the large-area main sensors after dicing measured at room temperature are shown in Fig. 7(a) and (b) with standard dicing and slim dicing, respectively.

Most of the sensors demonstrated no breakdown in leakage current up to 1000 V with the leakage current < 8 μA at 1000 V. Two sensors with standard dicing exhibited microdischarge (MD) breakdown at approximately 750 V, which is still above

the specification of MD breakdown >600 V. The ATLAS12M sensors with slim dicing show a tendency for an increasing leakage current above an onset voltage of approximately 800 V, while the ATLAS12M sensor with standard dicing and the ATLAS12A sensor with slim dicing do not. The observed differences may have arrived from subtle differences in the wafer lots and the fabrication processes. Inclusion of the slim dicing, the gated PTP structure, and the ganging has not deteriorated the initial performance of the large-area sensors.

An upward bump in the leakage current is observed at onset voltages of approximately 200 V for the ATLAS12M sensors and approximately 300 V for the ATLAS12A sensors. These onset voltages are corresponding with the full depletion voltages observed in Fig. 8, but independent of the edge space of the standard or slim dicing. The effect would be a surface generated current in the backside silicon–metal barrier associated with depletion of the backside implantation when the depletion had reached the backside.

4.2. Characteristics of wafers

Characteristics of wafer such as resistivity are evaluated by using $8\times8\,\mathrm{mm}^2$ square diodes from the ATLAS12A and ATLAS12M wafers, implemented at four places near edge of wafer, denoted by P1–P4 in Fig. 3. The resistivity of the wafer, ρ, can be calculated from the following equation:

$$\rho = W^2/(2\,\mu\epsilon V_{FD}) \tag{1}$$

$$\approx 10.6\times(W(\mu\mathrm{m}))^2/(V_{FD}(\mathrm{V}))\ (\Omega\,\mathrm{cm}) \tag{2}$$

where W is the active thickness of the diode at full depletion, V_{FD} is the full depletion voltage, μ is the charge carrier mobility for p-type wafer ($450\,\mathrm{cm}^2\,\mathrm{V}^{-1}\,\mathrm{s}^{-1}$) and ϵ is the dielectric constant of silicon ($11.9\epsilon_0=1.05$ pF/cm).

The full depletion voltage, V_{FD}, can be estimated from the measurement of the capacitance of the diode as a function of the bias voltage. The capacitance increases as the depletion region expands as a function of bias voltage and saturates once the diode is depleted fully. Since the capacitance of diode is

$$C\propto 1/w\propto 1/\sqrt{V} \tag{3}$$

where w is the depletion depth, the V_{FD} can be estimated from the cross point of two straight lines of the $1/C^2$ curve as a function of the bias voltage; one in the depletion expansion and the other in the depletion saturation.

The active thickness W can be estimated from the saturation capacitance. By assuming the active area of the diode being $6.6\times6.6\,\mathrm{mm}^2$ with a lateral depletion of 300 μm outside the diode implantation once it is fully depleted, the capacitance is calculated to be 14.3 pF for a thickness of 320 μm. The capacitance of a thickness W (μm) would be

$$C\sim14.3\times(320/W(\mu\mathrm{m}))\ (\mathrm{pF}) \tag{4}$$

and its inversion squared is

$$1/C^2\sim4.9\times10^{-3}\times(W\,(\mu\mathrm{m})/320)^2\ (\mathrm{pF}^{-2}). \tag{5}$$

The bias voltage dependence of the capacitance of the diodes was measured with a LCR meter at a frequency of 1 kHz [22]. The

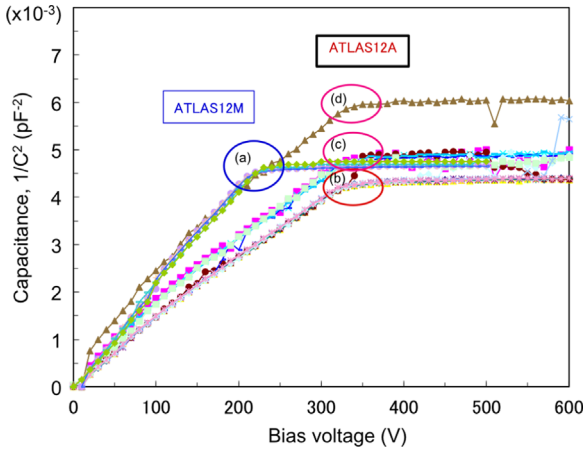

Fig. 8. Capacitances of the diodes of $8\times8\,\mathrm{mm}^2$ from ATLAS12A (b–d) and ATLAS12M (a) wafers as a function of bias voltage measured at a frequency of 1 kHz.

Table 2
Wafer parameters as derived from the capacitance of $8\times8\,\mathrm{mm}^2$ diodes.

Group	Sample id's	$1/C^2$ ($10^{-3}\,\mathrm{pF}^{-2}$)	C (pF)	W (μm)	V_{FD} (V)	ρ (k Ω cm)
(a)	ATLAS12M wafers W03, 07, 08	~4.68	~14.6	~313	~225	~4.5
(b)	ATLAS12A wafers W602-P1, P2, P4 W623-P1, P4; W648-P3,P4	~4.38	~15.1	~303	~330	~2.9
(c)	ATLAS12A wafers W602-P3, W623-P2, P3 W648-P1	~4.88	~14.3	~320	~330	~3.3
(d)	ATLAS12A wafer W648-P2	~6.02	~12.9	~355	~330	~4.0

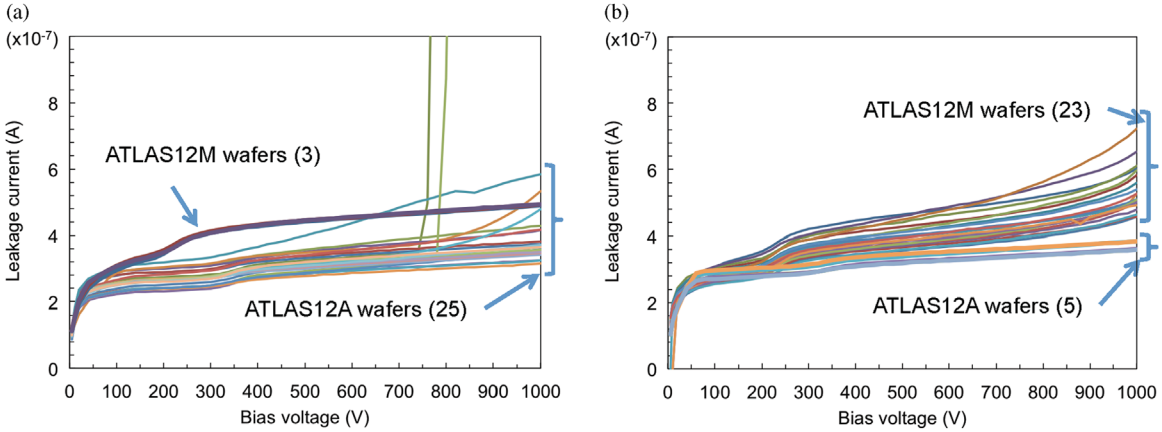

Fig. 7. Leakage currents as a function of bias voltage of the ATLAS12A and ATLAS12M large-area main sensors after dicing: (a) standard dicing and (b) slim dicing.

capacitances, $1/C^2$, are shown in Fig. 8 as a function of bias voltage. The samples from the ATLAS12M wafers are in the group (Fig. 8 (a)). Those from the ATLAS12A wafers are scattered in three groups (Fig. 8(b)–(d)). The diodes of the ATLAS12A wafers were sampled from wafers W602, W623, and W648. No noticeable systematic dependence on the wafers nor in the position of the diodes is apparent from the groups and the sample id's as in Table 2. The source of the observed systematic deviations is as yet unknown.

From Fig. 8, the full depletion voltages of the ATLAS12A and ATLAS12M wafers are V_{FD} approximately 330 V and 225 V, respectively. With the full depletion voltage V_{FD} and the active thickness W from the capacitance C at saturation, the resistivity ρ are derived and summarized in Table 2. The resistivity of the ATLAS12A and ATLAS12M wafers is approximately 3 and 4.5 k Ω cm, respectively.

The sensor manufacturer has confirmed the usage of different batch of wafers that are traced to come from different ingots. The homogeneity of resistivity at edge is confirmed with the measured data of the diodes. The resistivity over the wafer, the difference between center and edge, is measured by the wafer manufacturer in sampled wafers. The full depletion voltage of ATLAS07 wafer is approximately 200 V and is consistent with the ATLAS12M wafers.

5. Summary

We have been developing novel radiation-tolerant n^+-in-p silicon microstrip sensors for very high radiation environments, aiming for an application in the inner tracker of the ATLAS detector upgrade for the HL-LHC. Radiation tolerance has been studied with ATLAS07 sensors and with independent structures. Incorporating the results obtained for the minimum edge space for holding 1 kV bias voltage and the novel concept of "gated" PTP structure, the ATLAS07 design is developed into new ATLAS12

Table 3
Miniature sensors with or without a PTP structure and their position in ATLAS12 wafer layouts. Identifiers are, B for miniature sensors of axial geometry with a strip pitch of 74.5 μm, Z1 for narrow PTP gap (10 μm) without p-stop isolation, Z2 for individual p-stop, Z3 for default geometry, Z4 for atoll-type PTP structure, Z6 for wide strip pitch of 100 μm, EC for endcap sensors of stereo-strip fan geometry, EC-small pitch for square stereo sensor with a strip pitch of 64–65 μm, EC-large pitch for square stereo sensor with a strip pitch of 102–105 μm, EC-skewed: skewed stereo sensor with a strip pitch of 65–71 μm.

Id		ATLAS12A		ATLAS12M	
		PTP	No PTP	PTP	No PTP
BZ1		–	1, 11	–	7, 19
BZ2C		–	–	2, 14	–
BZ3A		–	–	1, 13	–
BZ3B		–	–	3, 15	–
BZ3C		2, 4, 12, 14, 15		6, 18	–
BZ3C-unpassivation		6, 16	–	–	–
BZ3D		–	–	9, 20	–
BZ3E		–	–	–	10
BZ3F		–	3, 5, 13	–	11
BZ4B2		–	–	4, 16	–
BZ6C		–	–	5, 12	–
BZ6E		–	–	–	8, 17
EC-small pitch-C	AC gang	7	–	–	–
	DC gang	17	–	–	–
	No gang	–	–	21, 23	–
EC-small pitch-E	AC gang	–	8	–	–
	DC gang	–	18	–	–
	No gang	–	–	–	22, 24
EC-large pitch-C	AC gang	9	–		
	DC gang	19	–	–	–
EC-large pitch-E	AC gang	–	10	–	–
	DC gang	–	20	–	–
EC-skewed-C		21	–	–	–
EC-skewed-E		–	22	–	–

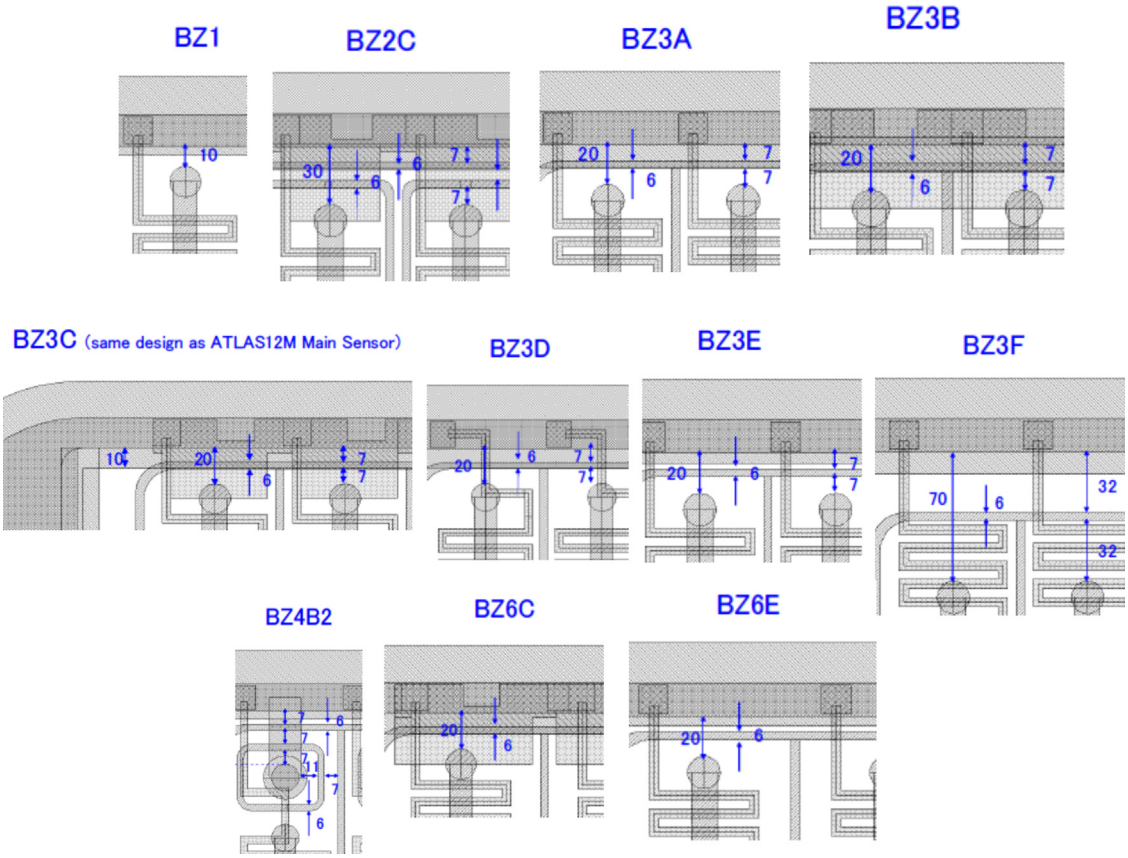

Fig. 9. Miniature sensors of axial geometry with or without a PTP structure in ATLAS12 wafers.

designs. The ATLAS12A large-area main sensor has 4 strip-segments of all axial geometry for prototyping an axial strip sensor. The ATLAS12M main sensor has stereo-strip segments for prototyping a stereo strip sensor. New to the ATLAS12 layouts are two dicing lines: standard edge space of 910 μm and slim edge space of 450 μm, a gated PTP structure at the end of strips, and connection of orphan strips to readout strips in a triangular corner of the stereo-strips segment.

The wafer processing of 120 ATLAS12A and 45 ATLAS12M wafers is completed using wafer lots of 6 in., p-type, FZ, and 320 μm thick. Out of these wafers, 30 ATLAS12A and 26 ATLAS12M wafers are diced to this report, resulting in 28 large-area main

Table 4
ATLAS12 miniature sensors of axial geometry, BZ1–BZ6.

Inner dimension of bias ring length × width (area)		8.14 × 7.82 mm^2 (0.637 cm^2)
Number of strips BZ1 – BZ4/BZ6		104/77
Strip pitch BZ1 – BZ4/BZ6		74.5/100 μm
Strip width of implant/metal		16/22 μm
Id	Strip length (mm)	Features
BZ1	8.06	No p-stop, PTP gap 10 μm
BZ2C	8.04	Individual p-stop, full gate-slit
BZ3A	8.05	Common p-stop, half gate-continuous
BZ3B	8.05	Common p-stop, full gate-continuous
BZ3C	8.05	Common p-stop, full gate-slit
BZ3D	8.05	Common p-stop, bias resistor gate
BZ3E	8.05	Common p-stop, no gate
BZ3F	8.00	Common p-stop, PTP gap 70 μm
BZ4B2	8.00	Common p-stop, PTP dot+bias resistor gate
BZ6C	8.05	Common p-stop, full gate-slit
BZ6E	8.05	Common p-stop, no gate

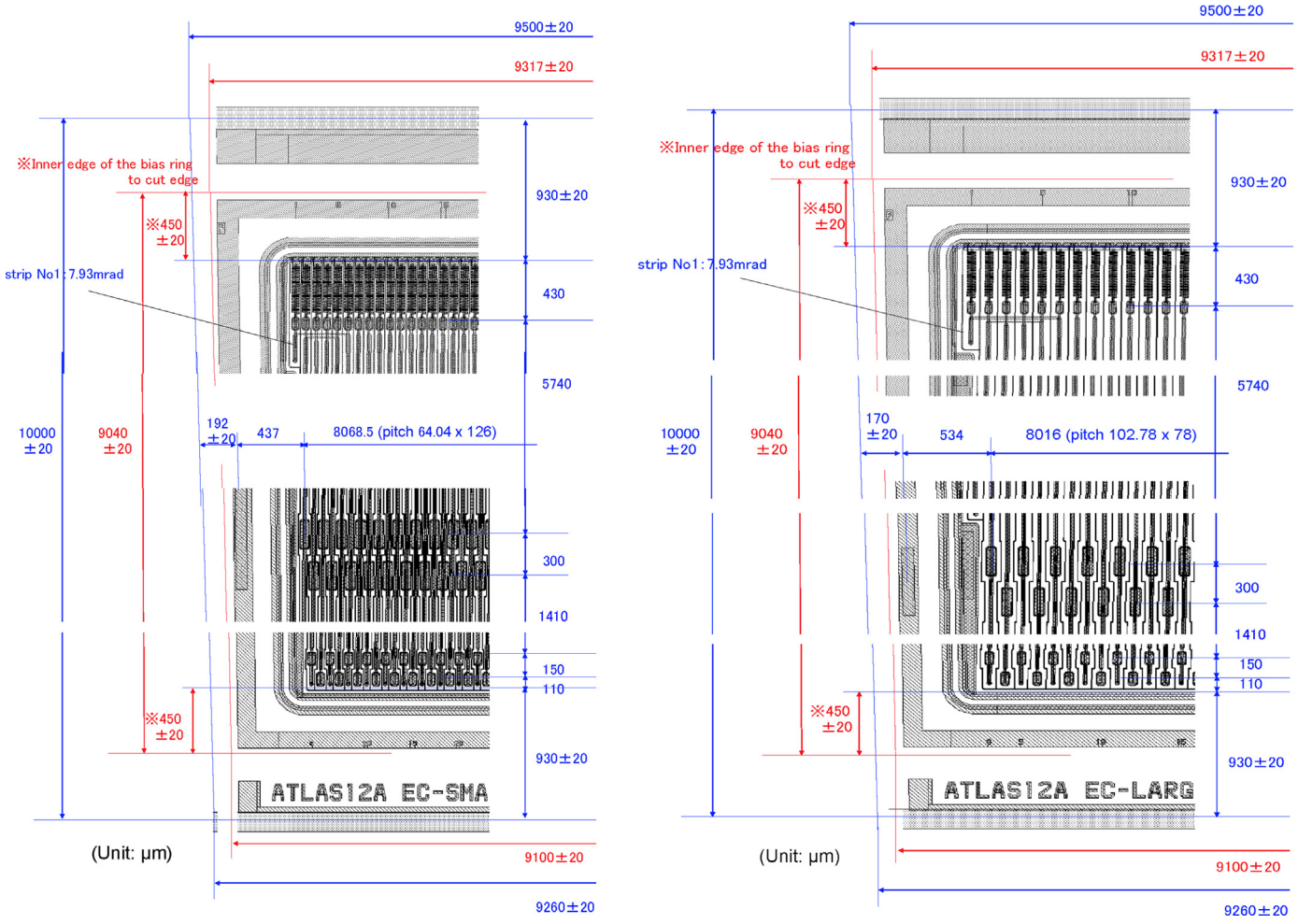

Fig. 10. Excerpts of the layout of endcap "square" stereo miniature sensor of fan geometry in the ATLAS12A wafer layout with narrow strip pitch (left figure) and wide strip pitch (right figure). The orphan strips at the top-left corner are connected to neighboring strips.

Table 5
ATLAS12 endcap miniature sensors of fan geometry.

Endcap "square" stereo miniature sensor with small strip pitch (EC-small pitch)	
Inner dimension of bias ring length × wide/narrow width (area)	8.14 × 8.52/8.33 mm^2 (0.686 cm^2)
Number of strips at wire-bonding pads	127
Strip length (θ: stereo angle)	8.05/cos θ mm
Strip pitch wide/narrow	65.06/63.55 μm
Angle, θ, of stereo strips	20 mrad
Endcap "square" stereo miniature sensor with large strip pitch (EC-large pitch)	
Inner dimension of bias ring length × wide/narrow width (area)	8.14 × 8.58/8.37 mm^2 (0.690 cm^2)
Number of strips at wire-bonding pads	79
Strip length (θ: stereo angle)	8.05/cosθ mm
Strip pitch wide/narrow	104.69/102.05 μm
Angle, θ, of stereo strips	20 mrad
Endcap "skewed" stereo miniature sensor (EC-skewed)	
Inner dimension of bias ring length × wide/narrow width (area)	17.68 × 18.38/16.73 mm^2 (3.10 cm^2)
Number of strips per segment	258
Top segment	
Strip length	8.77 mm
Strip pitch wide/narrow	70.98/67.90 μm
Bottom segment	
Strip length	8.80 mm
Strip pitch wide/narrow	67.67/64.60 μm
Skew angle	20 mrad

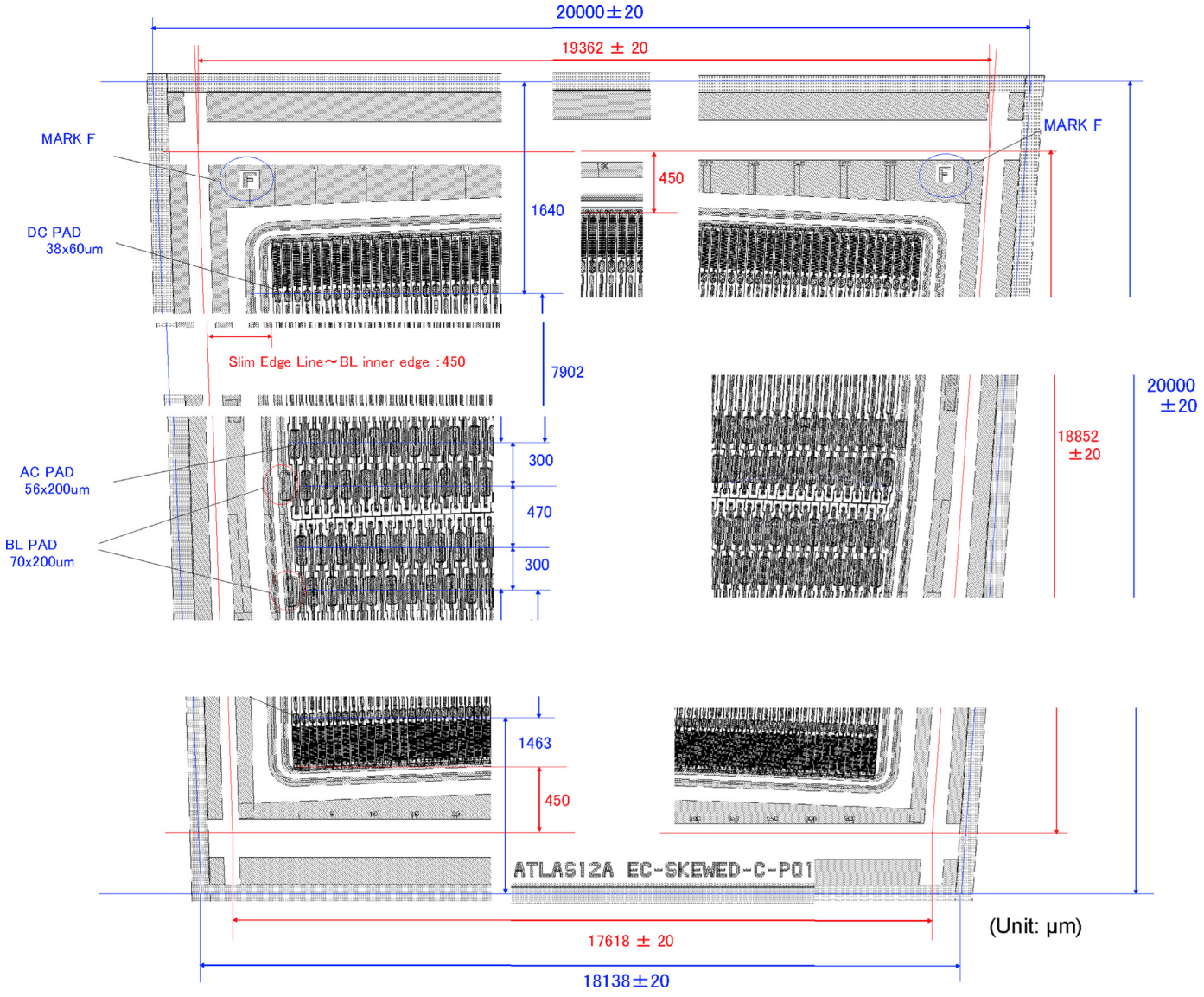

Fig. 11. Excerpts of the layout of endcap "skewed" miniature sensor of fan-geometry in the ATLAS12A wafer layout.

sensors of standard and 28 of slim dicing. Most of the sensors exhibit no breakdown in leakage current up to 1000 V. The leakage currents are $<8\,\mu A$ at 1000 V, measured at room temperature. Inclusion of the new features has not deteriorated the initial performance of the large-area sensors. By using capacitance measurement of the diodes, the full depletion voltages of the ATLAS12A and the ATLAS12M wafers are approximately 330 V and 225 V, and the resistivity of the wafers is derived to be approximately 3 and 4.5 k Ω cm, respectively.

Acknowledgments

The research was partly supported by the Ministry of Education, Youth and Sports of the Czech Republic (Grant number LG13009), the German Federal Ministry of Education and Research, and the Helmholtz Association, the Japan Society for Promoting Science KAKENHI A (Grant number 20244038) and KAKENHI C (Grant number 20540291), the Japan MEXT KAHENHI for Research on Priority Area (Grant number 20025007) and for Scientific Research on Innovative Areas (Grant number 23104002), the Slovenian Research Agency, the Spanish National Program for Particle Physics (under Grants FPA2009-13234-C04-01 and FPA2012-39055-C02-01), the financial support of the State Secretariat for Education, Research, and Innovation, the Swiss National Science Foundation and the Canton of Geneva, Switzerland, the UK Science and Technology Facilities Council (under Grant PP/E006701/1), and the United States Department of Energy, Grant DE-FG02-04ER41286.

Appendix A. Miniature sensors in the ATLAS12 wafer layouts

The ATLAS12A and ATLAS12M wafer layouts (Fig. 3) include miniature sensors composed of 20 $1\times1\,cm^2$ and two $2\times2\,cm^2$ sensors and 24 $1\times1\,cm^2$ sensors. Two dicing lines, the standard and slim dicing, are implemented as in the case of the main sensor. These miniature sensors are to be used for understanding and optimizing the designs against radiation damage further.

A.1. PTP structure variants

Variation of "gated" PTP structures is implemented in the miniature sensors of ATLAS12A and ATLAS12M wafers. Those structures in the miniature sensors of axial-strip geometry are shown in Fig. 9. The strip pitch, the PTP gap between strip end and bias ring, and the strip isolation method are 74.5 μm, 20 μm, and common p-stop, respectively, other than the strip pitch of 100 μm in BZ6C and BZ6E. Identification of the miniature sensor with and without a PTP structure and corresponding location per layout are summarized in Table 3.

The "full gate" structure (BZ3C) is the structure implemented in the main sensor. The "half gate" structure (BZ3A) where the gate is covering just over the p-stop structure is to compare with the "full gate" structures (BZ2C, BZ3B, BZ3C, BZ6C). The structures (BZ2C, BZ3C, BZ6C) have a "comb-like" slit at the corner of the p-stop structure to test whether the cut-out may improve the breakdown voltage while the sensor is reverse-biased. The structures (BZ3D, BZ4B2) with a "narrow and full gate" of the polysilicon bias resistor over the PTP gap are to test the difference in narrow and wide gate structures. The structures (BZ1, BZ3E, BZ3F, BZ6E) have no gate structure to compare with the gated structures. The BZ3F is the structure of the ATLAS07 main sensor. These variants may clarify the points in the structures susceptible to radiation damage. The geometrical specifications of the miniature sensors of axial geometry are summarized in Table 4.

A.2. Endcap "square" stereo miniature sensors

In order to arrange silicon strip sensors on discs of the endcap region, the sensor geometry must be trapezoidal and the strips must be laid in a fan geometry. A symmetrical geometry is a "square" trapezoid. In the same way as the stereo strips of the ATLAS12M main sensors, the strips in a fan geometry are inclined at an angle to the sensor edges to make a stereo sensor. An angle of 20 mrad is chosen so that the stereo angle of 40 mrad can be achieved with a pair of a stereo sensor. The radial strips can be arranged by rotating the pair of sensors by 20 mrad. Two types of these sensors are laid out with strips of small and large pitches: 64.04 μm and 102.78 μm at wire-bonding pads, respectively. Excerpts of the layout of the small and large pitch sensors are shown in Fig. 10. The ganging of orphan strips is made either by connecting the strip implants (DC-ganging) or connecting the AC-coupling strip metals (AC-ganging). The geometrical specifications of the endcap square stereo miniature sensors of fan geometry are summarized in Table 5.

A.3. Endcap "skewed" stereo miniature sensors

The orphan strips of the endcap square stereo sensors can be eliminated by arranging the sensor edges parallel to the stereo strips in a fan geometry. Consequently, the trapezoid is skewed at the inclination angle of the stereo strips. Excerpts of the layout of the endcap skewed stereo miniature sensor are shown in Fig. 11. The perimeters of the strip ends have been made circular, along with the row of wire-bonding pads, to prototype a circular sensor for accommodating a smooth transition in the radial transition region with a different quantization of the number of sensors in adjacent rings in a disc. The dicing lines of the miniature sensors are kept straight for this fabrication for simplicity. The sensor is positioned in a $2\times2\,cm^2$ area in the ATLAS12A wafer layout. The geometrical specifications of the endcap skewed stereo miniature sensors of fan geometry are summarized in Table 5.

A.4. Special miniature sensor without passivation

A very special sensor, labeled by BZ3C-unpassivation in Table 3, is a sensor where the edge region between the guard ring and the edge metal is without SiO_2 passivation. This is to make dicing at a point immediately outside of the guard ring, e.g., by the scribe and cleave technology [23].

References

[1] ATLAS collaboration, Journal of Instrumentation 3 (2008) S08003.
[2] ⟨http://hilumilhc.web.cern.ch/HiLumiLHC/index.html⟩.
[3] ATLAS collaboration, Letter of Intent for the Phase-II Upgrade of the ATLAS Experiment, CERN-LHCC-2012-022, LHCC-I-023.
[4] S. Baranov, et al., Atlas Radiation Background Task Force Summary Document, ATL-GEN-2005-001.
[5] S. Terada, et al., Nuclear Instruments and Methods in Physics Research Section A 383 (1996) 159.
[6] Y. Unno, et al., Nuclear Instruments and Methods in Physics Research Section A 636 (2011) S24.
[7] K. Hara, et al., Nuclear Instruments and Methods in Physics Research Section A 636 (2011) S83.
[8] J. Bohm, et al., Nuclear Instruments and Methods in Physics Research Section A 636 (2011) S104.
[9] S. Lindgren, et al., Nuclear Instruments and Methods in Physics Research Section A 636 (2011) S111.
[10] Y. Takahashi, et al., Nuclear Instruments and Methods in Physics Research Section A 699 (2013) 107.
[11] Cyclotron and Radioisotope Center (CYRIC), Tohoku University, Aramaki-Aoba 6-3, Aoba-ku, Sendai-shi 980-8578, Japan.
[12] Karlsruhe Institute of Technology, Irradiation center, Hermann-von-Helmholtz-Platz 1, 76344 Eggenstein-Leopoldshafen, Germany.
[13] Paul Scherrer Institut (PSI), 5232 Villigen PSI, Switzerland.

[14] Reactor Infrastructure Centre, Jozef Stefan Institute, Jamova 39, 1000 Ljubljana, Slovenija.
[15] The signal is read on a low-noise ASIC and digitized on a 10-bit ADC. The measurements were made with a setting file "kazu.ini" that sets the front-end shaper peaking time to approximately 20 ns, ⟨http://www.alibavasystems.com/⟩.
[16] G. Lindstrom, et al., Nuclear Instruments and Methods in Physics Research Section A 426 (1999) 1.
[17] S. Mitsui, et al., Nuclear Instruments and Methods in Physics Research Section A 699 (2013) 36.
[18] Y. Unno, et al., Nuclear Instruments and Methods in Physics Research Section A 636 (2011) S118.
[19] Y. Unno, et al., Nuclear Instruments and Methods in Physics Research Section A 731 (2013) 183.
[20] ABC130 ASIC Specification v4.6, July 05, 2013, ATLAS internal document.
[21] M. Kumagai, et al., IEEE Transactions on Semiconductor Manufacturing 20 (2007) 259, ⟨http://www.hamamatsu.com/jp/en/technology/innovation/sd/index.html⟩.
[22] The bias voltage was provided with ADCMT R8340 power supply and the capacitance was measured with a LCR meter HP 4284A with a HP-custom-made high-voltage decoupling circuitry.
[23] V. Fadeyev, et al., Nuclear Instruments and Methods in Physics Research Section A 731 (2013) 260.